ORIGINAL PAPER

Evaluation of Optimal Design Parameters of the Geogrid Reinforced Foundation with Wraparound Ends Using Adaptive FEM

Sagar Jaiswal[1] · Vinay Bhushan Chauhan[1]

Abstract

This paper presents the numerical study based on the adaptive finite element analysis of the bearing capacity of a strip footing on reinforced soil mass. A parametric study has been conducted to estimate the ultimate load-bearing capacity of footing having a width, B resting over reinforced soil mass ($q_{ult, R}$) using wraparound ends configuration of geogrids. Based on the load-settlement response, the bearing capacity ratio (BCR) for all the studied wraparound ends configurations are evaluated, and their potential failure envelopes have been discussed. From the study, the optimum values of the wraparound end reinforcement geometrical configuration are noted as normalized width of reinforcement (b/B) = 3; depth of the first layer of reinforcing layer from the bottom of the footing to the width of footing ratio (u/B) = 0.25; normalized vertical spacing between successive layers of reinforcement (h/B) = 0.30; normalized vertical length of the wrapping ends (d/B) = 0.20; and the normalized lap length of wrapping ends of geogrid (l/B) = 0.50. The results noted from the study indicates that the axial elastic stiffness of the geogrid (EA) governs the ultimate bearing capacity of footing and the $q_{ult, R}$ is improved by almost 62% for settlement ratio (s/B) = 10%, upon reinforcing the soil mass with wraparound ends technique at EA = 5000 kN/m. This study also focuses on the normalized vertical stress (σ_{yy}/q_u) and normalized vertical strain (ε_{yy}/q_u) of the soil mass beneath the footing to investigate the influence of reinforcement on the soil mass beneath the footing.

Keywords Adaptive finite element method · Geogrid · Wraparound ends · Settlement · Ultimate load-bearing capacity · Strip footing

Introduction

Reinforcing the soil beds for enhancing the ultimate load-bearing capacity and/or reducing the anticipated settlement of the shallow foundation using geosynthetics has been extensively studied in the past and being adopted as a routine ground improvement technique for founding the various structures such as bridge abutments, embankments, and shallow foundations [1–15]. The technique of reinforcing the soil mass by placing the extensible reinforcement layers beneath the foundation is practiced to produce a composite foundation material with improved load-settlement performance characteristics. It is essential to estimate the actual load-bearing capacity and settlement of the foundation for safe, sustainable and imperative construction of superstructure over the foundations. However, for a given settlement value of a strip footing, the required reinforcement needed to maximize the improvement in the bearing capacity of the footing has not been established yet.

Though, many past studies have investigated the effect of material type and governing parameters of the reinforcement on the improvement of the load-settlement behavior of shallow foundations, by exercising the experimental and numerical approaches for wide-ranging relative densities of the soil mass. The modern concept of reinforced fill was presented by Vidal for a composite material manufactured from flat strips placed horizontally in a frictional fill, implying the interaction between the reinforcement and the soil by friction being merely generated by gravity [16]. The first systematic study to enhance the bearing capacity of a shallow foundation by reinforcing it with steel strip was carried out by Binquet and Lee [17]. Afterward, several studies were

✉ Vinay Bhushan Chauhan
  chauhan.vinaybhushan@gmail.com; vbcce@mmmut.ac.in

  Sagar Jaiswal
  sagarjaiswal.work@gmail.com

1 Civil Engineering Department, Madan Mohan Malaviya University of Technology, Gorakhpur 273010, Uttar Pradesh, India

conducted for improving the load-bearing capacity of a reinforced shallow foundation using fibers [18], metal strips [19, 20], geocell [21], geotextile [13, 22–27], and geogrid [4, 22, 28–35], as a reinforcing material.

The above-mentioned literature mainly discussed the effect of horizontal geosynthetics reinforcement on the bearing capacity of the footing over reinforced soil. Shukla's wraparound reinforcement technique addressed the situation of unavailability of land for laying the reinforcement on either side of the footing or the presence of property line nearby the footing and put forward the concept of wraparound ends technique of geosynthetic reinforcement [36]. Thereafter, it has been researched experimentally, analytically, and numerically by Kazi et al. [13, 26, 37] and Aria et al. [38]. In this technique, the ends of the reinforcing element are wrapped on both sides along the width, which also provides confinement to the soil mass. Nonetheless, the literature discussed above lacks an examination of vertical stresses, and strain up to the zone of influence of applied surcharge below the footing, in both unreinforced and reinforced situations.

In the recent studies, the improvement in the ultimate load-bearing capacity of the footing has been reported in the form of ratio between the ultimate load-bearing capacity of the reinforced ($q_{ult, R}$) to the unreinforced earth bed (q_{ult}) at the same settlement level and is known as bearing capacity ratio (*BCR*) [39–41]. Evaluation of the improvement in the bearing capacity of the foundation on reinforced sand beds was carried out using many small-scale experimental studies [32, 34, 42, 43] and it is worth to note that the stress distribution beneath the footing resting on a reinforced soil is affected by the location of reinforcement [44]. Though the experimental studies were incompetent to describe the stress–strain behavior of the reinforced soil at desired locations, and simultaneously being time-consuming and costlier. In such circumstances, numerical studies using various advanced approaches (such as finite element method (FEM), discrete element method (DEM), and finite difference method (FDM)) are found to be appropriate for analyzing the load-settlement behavior and also help to understand the soil-structure interaction between the soil and geosynthetic reinforcement [13, 26, 32, 45–47].

Despite the fact that FEM/FDM/DEM can be used proficiently to model the soil behavior, it remains a challenging task to overcome the discontinuities in the numerical model that can occur during the iteration of the simulations. The scenario described above is critical in controlling the interaction systems of soil structure, such as soil particle erosion near the subsurface system [48] and the interlocking of soil and geogrid [49].

In view of the foregoing, this study aims to utilize FEM to evaluate the optimum parameters of wraparound ends configuration of reinforcement viz., width of the geogrid (*b*),

placement of the first layer from the bottom of the footing (*u*), vertical spacing between two consecutive reinforcing layers (*h*), lap length (*l*), and vertical distance of the overlapping length (*d*) for a footing with width, *B* resting over reinforced soil mass. The variation in the development of the potential failure plane below the footing due to the change in the above-mentioned parameters has been discussed to examine the influence of geogrid configuration on the load-settlement response of the footing resting over the reinforced and unreinforced earth beds. A thorough discussion on the normalized vertical stress (σ_{yy}/q_u) and normalized vertical strain (ε_{yy}/q_u) has been done, and the influence of wraparound ends reinforcement on these parameters is examined.

Problem Statement

With reference to the discussion made in the previous section, a comprehensive parametric numerical study has been performed for a strip footing of width, $B = 4$ m, resting over the reinforced soil mass using a finite element method (FEM) based numerical tool, Optum G2 [50]. The numerical model with all the possible parametric combinations, as shown in Fig. 1, has been simulated to obtain the optimum geometrical configurations of geogrid reinforced for a 4 m wide strip footing. All the reinforcement configurations of the wraparound end technique used in the present study are shown in Fig. 2. The reinforcing parameters of the wraparound ends (i.e., discussed in the following section) have been varied to examine their effect on the load-settlement characteristics and development of potential failure envelopes below a strip footing under uniformly distributed multiplier load resting over the reinforced foundation.

The simulated models were analyzed for the reinforced cases to compare with the unreinforced one, and additionally to obtain the optimum parameters that contribute to the $q_{ult, R}$ of the foundation in case of reinforcement using geogrid. Extensive numerical models were simulated to examine the behavior of the footing under the various geometrical configurations of geogrid and obtained data were studied with the help of plots between various significant parameters. For $h/B = 0.30$, the reinforcement case $d/B = 0.30$ is not possible as the overlapping ends of the bottom layer will coincide with the horizontal reinforcement (i.e., *b*). This is the reason that simulations for $d/B = 0.30$ have only been performed for $h/B = 0.40$ condition (as shown in Fig. 1). The values of the b/B, u/B, h/B, d/B, and l/B have been considered suitably as per the recommendations available in the past studies [26, 29, 51–53], as mentioned in Fig. 1. Additionally, the impact of reinforcement on the stress and strain distributions in the foundation soil below the footing and all the potential failure
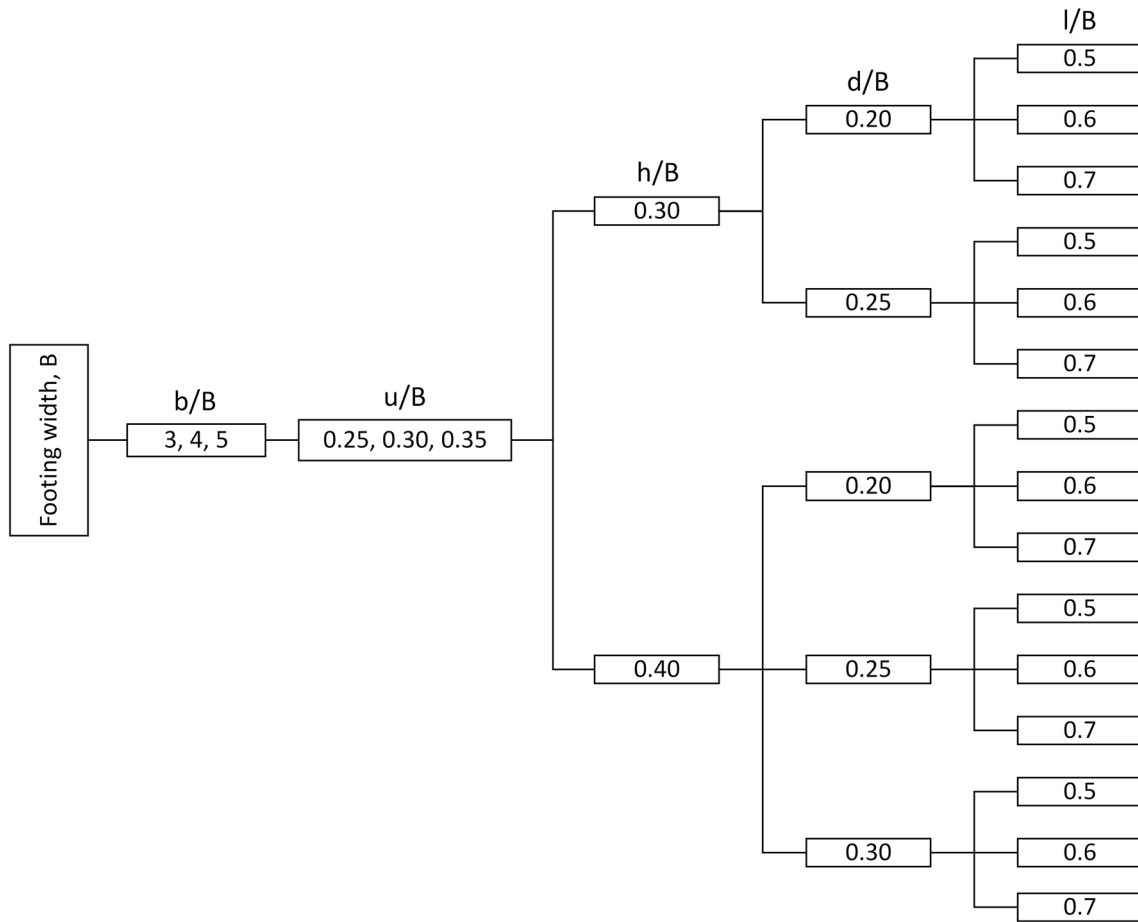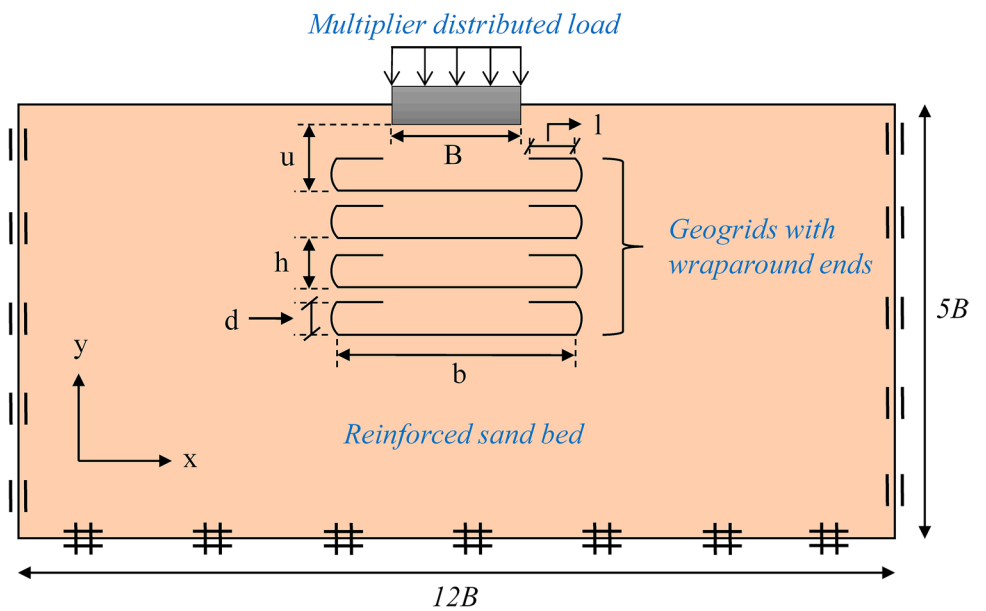
Fig. 1 Geometrical reinforcement configurations considered in the present study

Fig. 2 Material identification and model details (not to scale)

envelopes are investigated with the help of finite element simulations.

Numerical Modeling

Figure 2 shows the two-dimensional (2D) model of a footing resting over the reinforced cohesionless sand bed. The cohesionless soil is modeled as a material following the Mohr–Coulomb yield criterion with the associated flow rule. Reinforcement layers are modeled using geogrid elements, which are one-dimensional axial members with no bending stiffness in the normal direction. The boundary conditions are shown in Fig. 2, where the vertical boundaries are restrained in the normal direction and the bottom horizontal boundary is restrained in both the vertical and horizontal directions.

Mesh size for the simulation of any problem should be considered large enough so that the shear failure zone of the footing should not get intercepted by the mesh boundaries. In absence of such situation, accuracy of the numerical model might be the compromised one. Considering the above, a number of trials have been performed and assimilated that for the present study and noted that the vertical and the horizontal (on either side) boundaries should be kept at 5 and 6 times the footing width (B), respectively, from the geometrical center of the footing (as shown in Fig. 2). All the material properties that have been taken into account for the present analysis are shown in Table 1.

Based on the recommendations available from the previous studies, the interface friction angle between the soil and geogrid is considered as two third of the internal friction angle of soil, i.e., $R_{int} = 2/3$ [26, 38, 41].

Total number of elements present in the mesh must be appropriate for the better convergence and higher efficiency of the numerical model [49]. Additionally, it is well-known that higher the total number of elements in the mesh, the higher will be the accuracy of the numerical model. However, taking a large number of elements for any mesh can be time-consuming, as it takes more time to converse the numerical results in each step of the simulations. Therefore, to overcome the

above situation, a sensitivity analysis on the total number of elements in the present mesh has been performed using adaptive finite element analysis [54–56], and 10,000 elements with a refinement factor of 0.25 are found suitable for the present study. The refinement factor of 0.25 essentially divides the number of elements into quarters, also the mesh refinement operations approximately quadruple the number of line elements and octuple the number of area elements (for the cases of geogrid and soil, respectively). If the generated mesh is found to be not suitable for the assessment of the ultimate bearing capacity within the required tolerance limit, then it can be refined again to obtain an appropriate mesh for the simulation. Furthermore, it is noted that the q_{ult} was found to be unaffected with a further increase in the total number of elements in the chosen mesh. The generated mesh and the discretization of elements are shown in Fig. 3. The type and size of elements considered in any analysis is an important aspect while performing the numerical analysis [57]. For a multiplier elastoplastic analysis, the recommended six-node Gauss element is used in the present study [41]. Numerical analysis for all the possible cases considered in this study was performed in plane strain conditions (strain in the direction normal to x and y, i.e., ε_{zz} is equal to 0). A feature available in the Optum G2 [50], termed as mesh fan (as shown in Fig. 3) is used at the bottom corners of the footing, to accommodate the maximum number of elements near the footing. This feature facilitates the further refinement of the surrounding elements and to have an insight into the potential shear failure plane and stress–strain distribution, an advantage over the small-scale laboratory or field tests.

In the present study, a multiplier elastoplastic analysis has been carried out to obtain the plots of load versus settlements of the strip footing. The multiplier elastoplastic analysis can be referred to as the combination of the limit analysis and the elastoplastic analysis where the numerical simulation is carried out at a regular step with deformation computed at each load in incremental step. The number of elastic steps (N_E) and plastic steps (N_P) can be defined manually to converge the results rapidly. Considering a typical load–displacement response as shown in Fig. 4, the curve will initially be approximately linear and then gradually become more and more curvilinear. The values of N_E and N_P have been studied and it is observed that any increment in these values leads to more refined and accurate results of ultimate load-bearing capacities, however, $N_E = 10$, and $N_P = 10$, are found to be good enough to produce precise results. In this study, iterations using three adaptive steps are implemented, in such a manner that each adaptivity iteration starts from 1000 elements and ends at 10,000 elements until the final solution is attained.

Table 1 Material properties considered for the present study

Properties	Soil	Reinforcement	Footing
Modulus of elasticity, E (MPa)	30	–	–
Poisson's ratio, ν	0.25	–	–
Cohesion, c (kPa)	0	–	–
Friction angle, ϕ (°)	25	–	–
Axial elastic stiffness, EA (kN/m) ($\times 10^3$)	–	1, 2, 5, 7, 8.5, 10	–
Unit weight, γ (kN/m³)	18	–	24
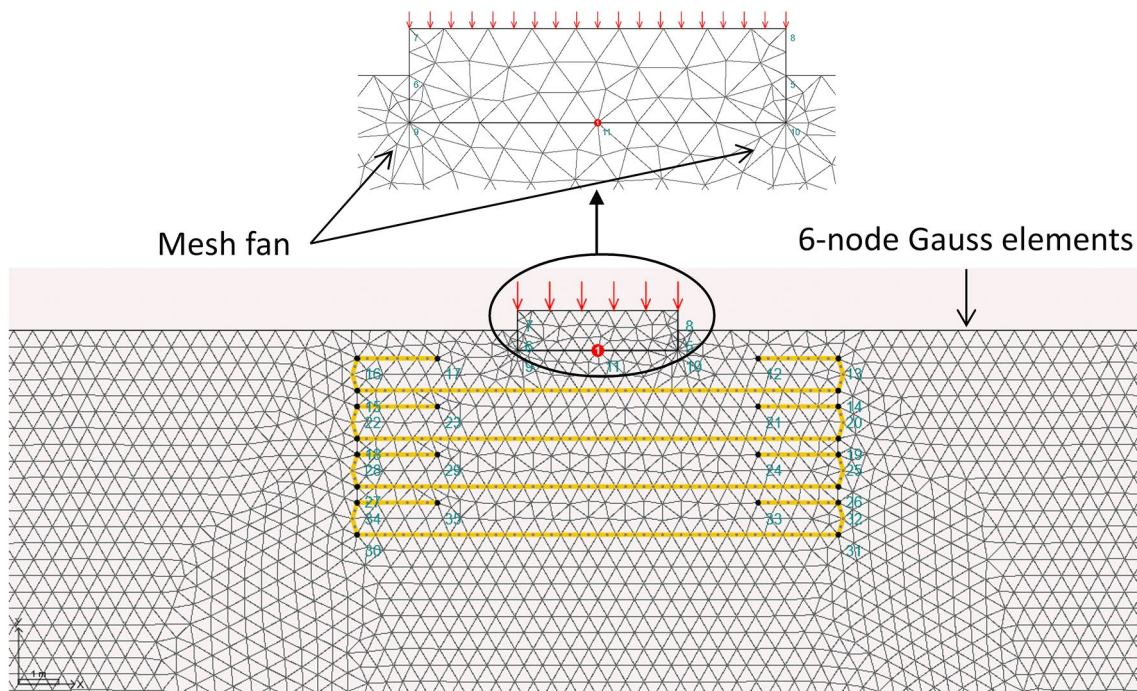
Fig. 3 A pictorial view of generated mesh and discretization of elements for the numerical model used in the present study

**Fig. 4** Load–displacement response for multiplier elasto-plastic analysis
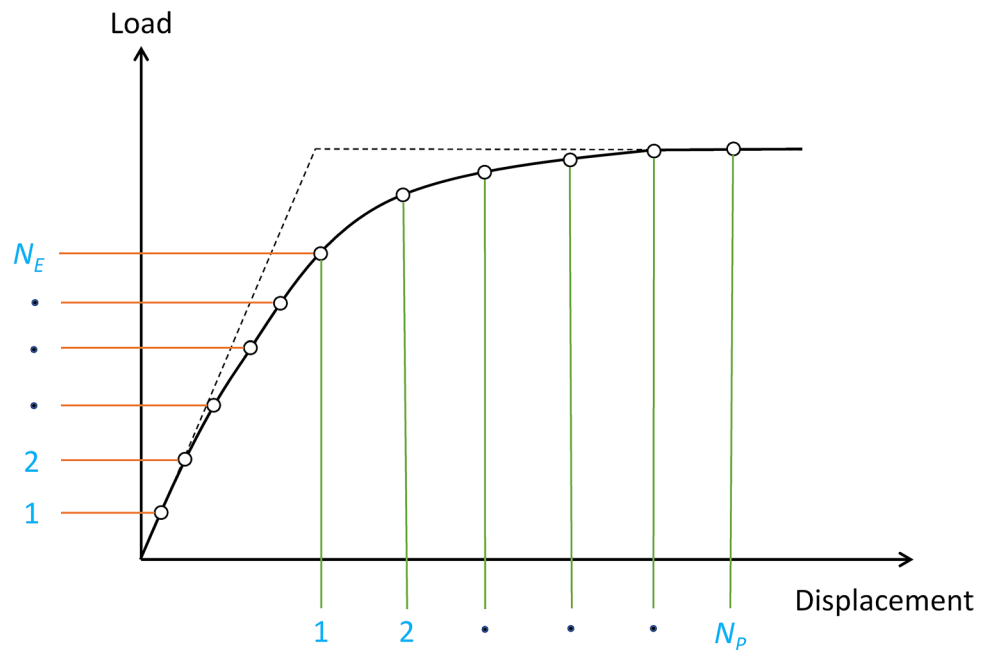
Results and Discussion

The load-settlement curves for all the cases of the footing mentioned in the previous section are obtained and discussed in the subsequent sections. The results of the parametric study for a 4 m wide strip footing have been presented to examine the effect of the reinforcing parameters namely, u/B, d/B, l/B, b/B, and h/B.

Figure 5 shows the variation of normalized reinforcement width (b/B) by keeping all the other reinforcing parameters constant (i.e., u/B, l/B, d/B, and h/B). The results showed that reinforcing the sand bed brings a substantial improvement in the bearing capacity of the foundation. It has been noted that there is not any common consensus on the reinforcement

**Fig. 5** Variation of load-bearing pressure versus settlement ratio for different width ratios, *b/B*
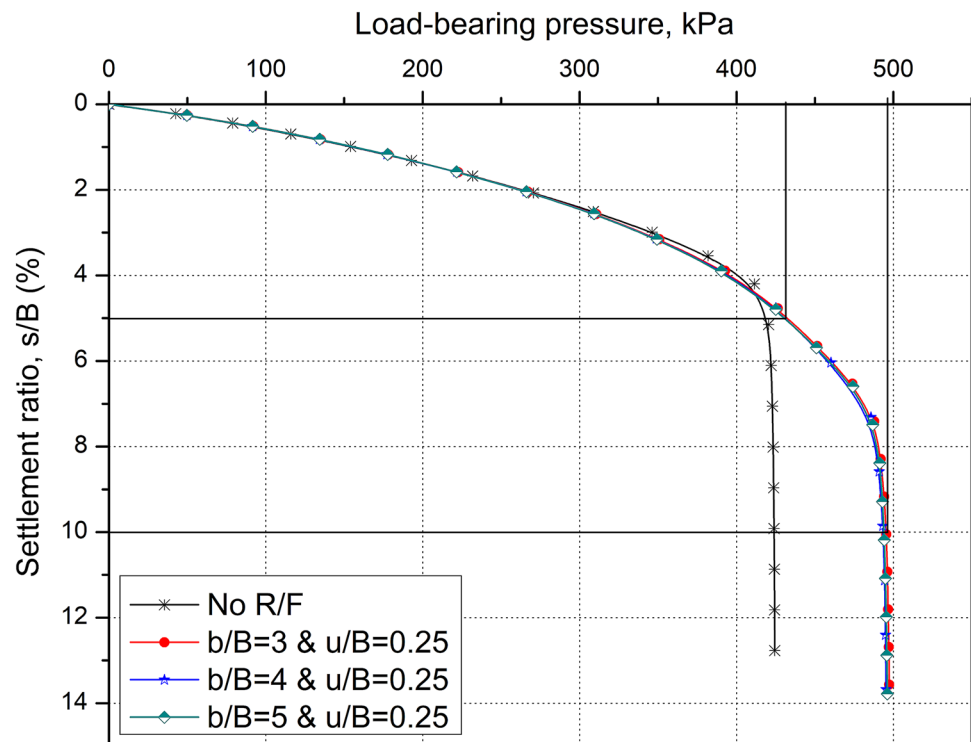
width (*b*) for maximizing the benefits of the reinforcement in terms of ultimate bearing capacity improvement of the footing among the findings of previous studies as the recommendation ranges from 4 to 8*B*, i.e., 4*B* [25, 58], 5*B* [58–60], 5–7*B* [24], 8*B* [29]. Nonetheless, in the present study, it is investigated that after reinforcing the soil mass using wraparound ends of geogrid, the trend variation remains constant on increasing the width ratio (*b/B*) from 3 to 5, and the load-settlement curves coincide with each other. The improvement in ultimate load-bearing capacity of reinforced sand bed ($q_{ult, R}$) at *s/B* = 10%, where *s* is the settlement of the footing, is found to be ranging from 16 to 18% for *b/B* = 3, 4, and 5, than that of the unreinforced condition (q_{ult}). No significant improvement in the *BCR* for *b/B* > 3 is noted due to the relocation of the wrapping ends situated far away from the footing ends. The above-noted observation leads to the conclusion that the distance between the wrapping ends of geogrid majorly affects the load-bearing capacity of the foundation.

Figure 6 depicts the variation in *BCR* corresponding to the normalized settlement ratio (*s/B*) of 5% and 10% as a function of the width of the reinforcing layer (*b/B*). It is noted that the *BCR* at different settlement ratios are constant up to *b/B* = 4 for *s/B* = 5% and beyond *b/B* = 4, an insignificant decrease in *BCR* is reported. Also, it decreases marginally for *s/B* = 10% with an increase in *b/B* from 3 to 5. This is possibly due to the fact that with the increase in the width of the geogrid, utilization of the wrapping ends cannot be done as they tend to move far away from the footing, which

could not effectively confine the mobilizing soil in the lateral direction of the reinforcement.

The movement of the soil mass under the applied load on the footing can be better understood by the potential shear failure envelope noted from the numerical analysis, which can be obtained from the shear dissipation plots for unreinforced and different cases of the reinforced soil mass, as shown in Fig. 7. The failure envelope of an unreinforced soil mass obtained in the present study (as shown in Fig. 7a) is similar to that identified by Terzaghi [61]. For reinforced condition, i.e., Fig. 7b, it is noted that the yielding of the soil is obstructed by the width (straight ends) and the wrapping ends of the geogrids, which tends to produce two-way confinement of the soil well within the reinforcement zone. This confinement restrains the mobilization of the soil mass by the high tensile load-bearing member beneath the footing, which confirms that geogrid reinforcement tends to bring an improvement in the settlement characteristics of the soil. However, Fig. 7c and d indicates that the wrapping ends of the geogrid do not intercept the failure envelope below the footing, which denotes that while increasing the width of the reinforcement from *b/B* = 3 to 5, no significant enhancement is observed. It indicates that *b/B* = 3 is the optimum width of the reinforcement for the considered case when reinforced with four layers of geogrid (*N* = 4, where *N* denotes the number of reinforcing layers). This finding of the optimum reinforcing layers is in line with the noted observation in an experimental study carried out by Buragadda and Thyagaraj [62].

Fig. 6 Variation in *BCR* with *b/B* at different normalized settlement ratios, *s/B*
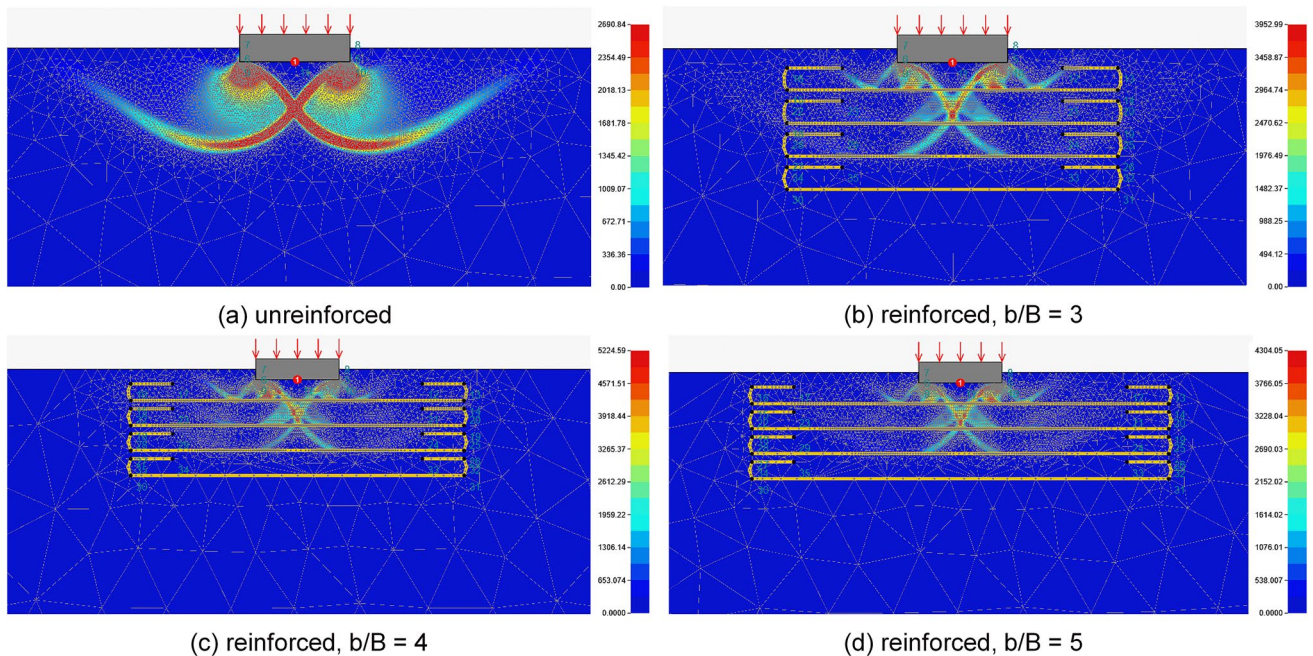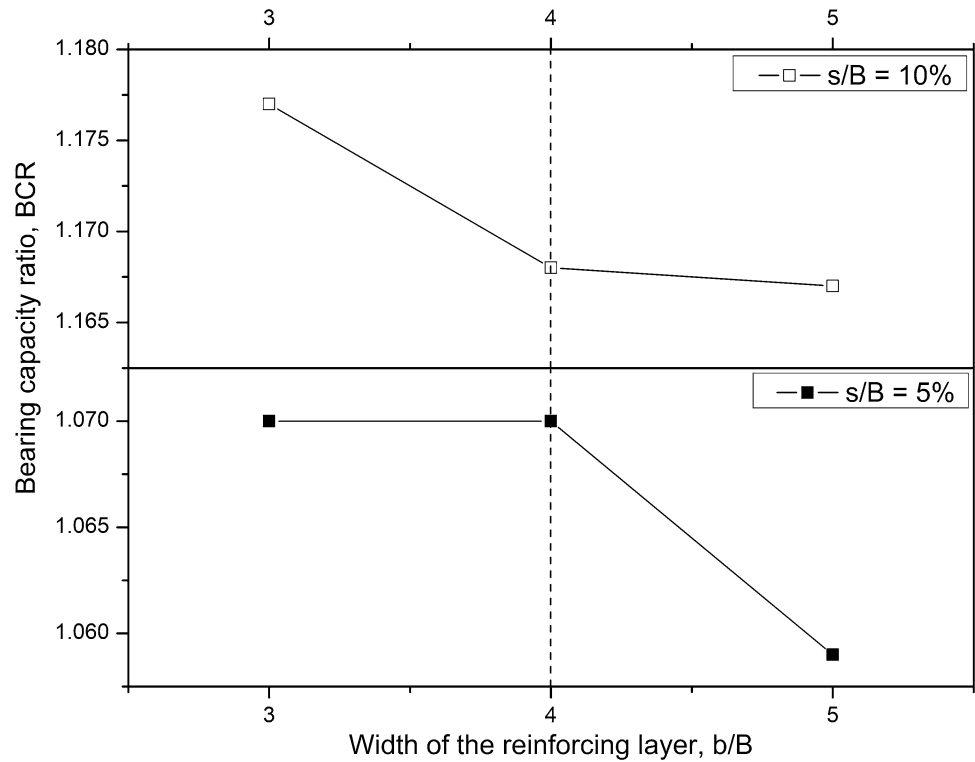

Fig. 7 Potential failure patterns for **a** unreinforced soil mass; **b** reinforced soil mass with *b/B* = 3; **c** reinforced soil mass with *b/B* = 4; and **d** reinforced soil mass with *b/B* = 5

Once finalizing the *b/B* = 3 as an optimum width of reinforcement, the effect of the depth of the first layer of reinforcement (*u/B*) is investigated. The parameter *u/B* has been varied in the range of 0.25–0.35 while keeping all the other parameters (i.e., *d/B*, *l/B*, and *h/B*) as invariable. The effectiveness of *u/B* can be noted in Fig. 8, where it is indicated that as the value of *u* increases from 0.25*B* to 0.35*B*, the improvement in the $q_{ult, R}$ decreases. The variation of the q_{ult}

Fig. 8 Variation of load-bearing pressure versus settlement ratio for various *u/B* ratios
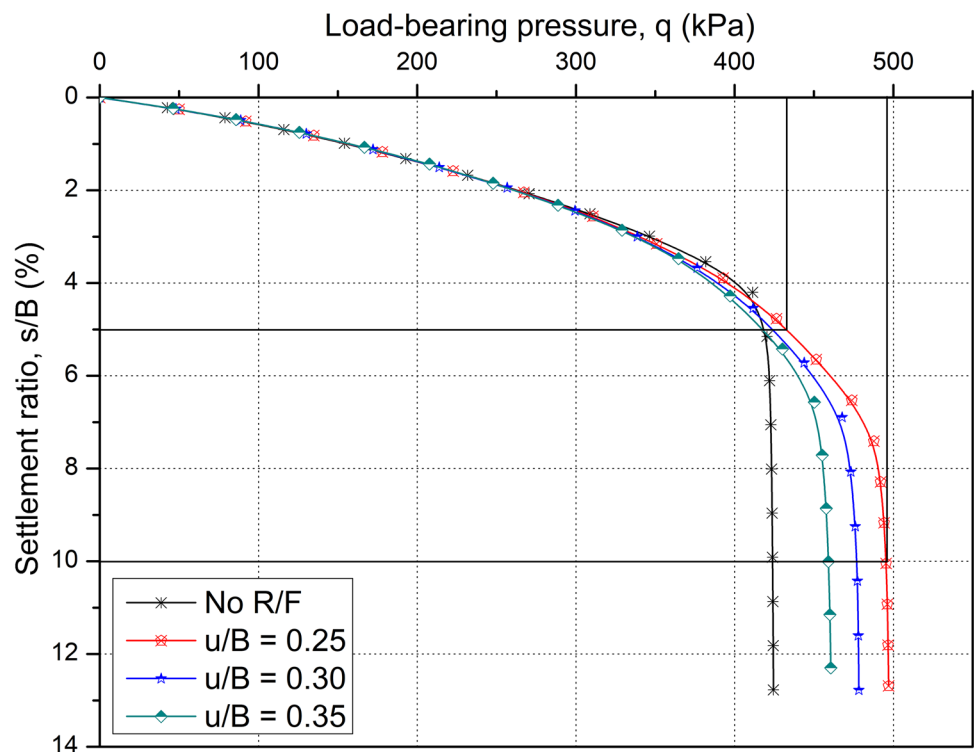
and $q_{ult, R}$ is almost linear for $s/B < 3\%$, and a drastic change is observed when $s/B > 4\%$, owing to the fact that the soil is in the plastic stage. The results show that by increasing the depth of the first layer of reinforcement (*u/B*) at 0.25, 0.30, and 0.35, the improvement in $q_{ult, R}$ is noted as 17.6%, 12.8%, and 8.5%, respectively at settlement ratio, $s/B = 10\%$. Previously, former studies noted that the depth of the first layer of reinforcement (*u*) with straight ends are 0.3*B* [20], 0.33*B* [19], 0.375*B* [28], however, this study recommends an appropriate *u* of 0.25*B* for significant improvement in the $q_{ult, R}$, which is similar to the findings reported by Adams and Collin [52]. Moreover, the bearing capacity ratio (*BCR*) diminishes with the increase in the depth of the first reinforcing layer from the bottom of the footing. The variation of the *BCR* with *u/B* ratio at different *s/B* ratios is compared and shown in Fig. 9. For the present study, it is noted that *BCR* is marginally reduced by 2.2% and 4.6% at $s/B = 5\%$ and 10%, respectively, when *u/B* changes from 0.25 to 0.30. Additionally, a reduction of 4.6% and 8.8% in the *BCR* is observed when *u/B* changes from 0.25 to 0.35 for normalized settlement ratio, $s/B = 5\%$ and 10%, respectively.

For a better understanding of the results for variation in the depth of the first layer of reinforcement (*u/B*), the potential failure envelopes for reinforced and unreinforced cases are compared using shear dissipation plots and shown in Fig. 10. The findings of the present study show that the better usage of reinforcing material can be achieved when the reinforcement zone exists between 1.5 and 1.8 times the footing width (*B*), whereas earlier researchers reported the

effective reinforcement zone as 1.5*B* [20], 1.6*B* to 2.2*B* [63]. The potential failure envelope presented in Fig. 10, illustrates that as the *u/B* ratio increases, the effectiveness of the third and fourth layers of reinforcement dissipates. Figure 10b indicates that the shear failure region is well within the zone of reinforcement, and all the layers of reinforcement are taking part in the improvement of load-settlement characteristics of the footing. Nevertheless, in Fig. 10c and d, it is evidently visible that only the first two layers are participating in supporting the load transferred by the footing to the soil. From the failure patterns obtained for the variation of *u/B* ratio, it can be concluded that for the maximum utilization of the reinforcing element, the reinforcement must be placed amply within the zone of failure.

Previously, researchers showed in their studies that the spacing between the successive layers of geogrids also governs the load-settlement characteristics of the footing, and beyond a certain spacing between the successive layers, the effect of the reinforcement diminishes [28, 29, 52]. To examine the effect of reinforcement with wraparound ends with respect to the unreinforced foundation bed, the spacing between successive layers is varied to understand the load-settlement response of the footing. The geogrid reinforcement width and the depth of the first layer of geogrid are kept constant at $b/B = 3$, and $u/B = 0.25$, as at these values, the improved *BCR* is highest among the studied ones. Additionally, *d/B* and *l/B* are also kept invariable, whereas *h* is varied at 0.30*B*, and 0.40*B*, respectively. Figure 11 indicates that the $q_{ult, R}$ decreases with the increasing magnitude of *h*.

Fig. 9 Variation of *BCR* with *u/B* at *s/B* = 5% and 10%
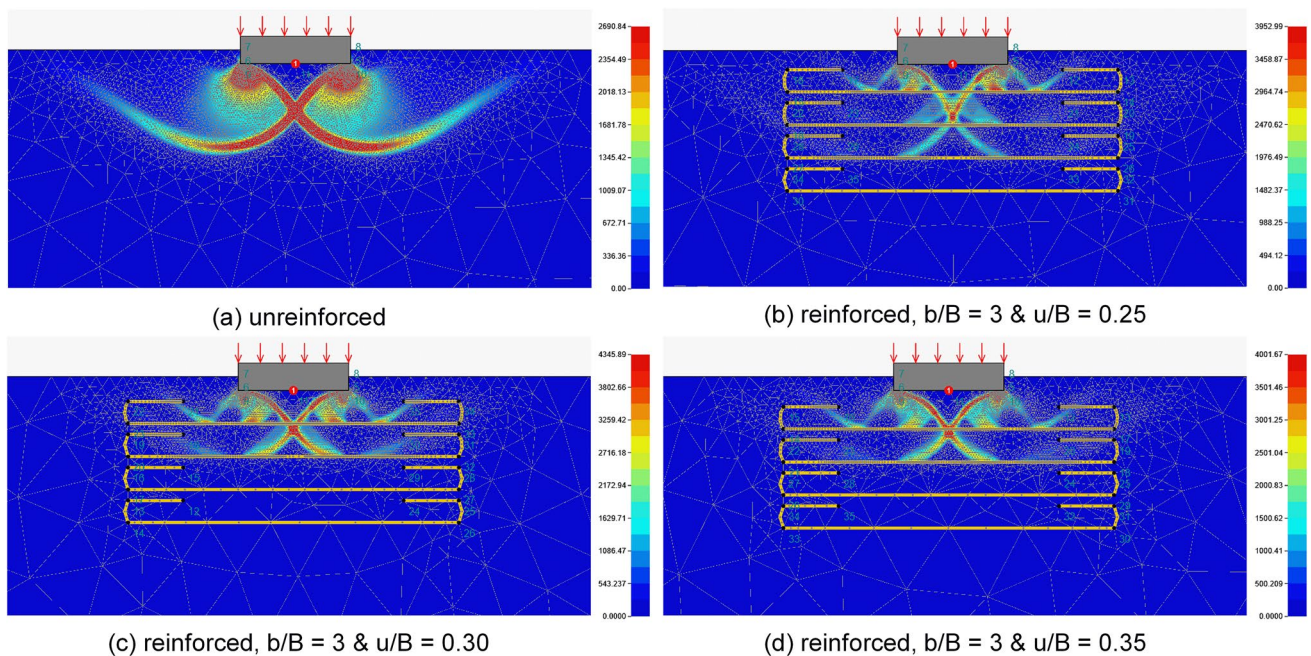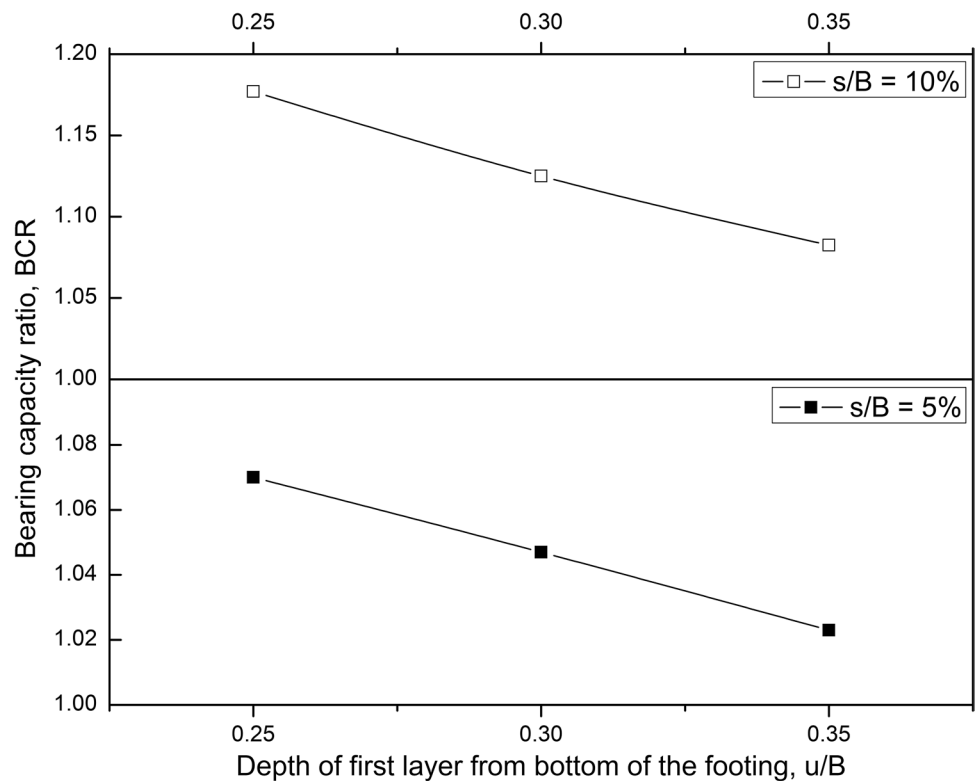

Fig. 10 Potential failure patterns for **a** unreinforced soil mass; **b** reinforced soil mass with *b/B* = 3 & *u/B* = 0.25; **c** reinforced soil mass with *b/B* = 3 & *u/B* = 0.30; and **d** reinforced soil mass with *b/B* = 3 & *u/B* = 0.35

An improvement of 17.8% and 10% at *h/B* = 0.30 and 0.40, respectively, is noticed in the $q_{ult, R}$ than the q_{ult} but a reduction of 6.4% in the $q_{ult, R}$ is registered when *h/B* varies from 0.30 to 0.40. In view of the above, this study recommends

the optimum value of *h/B* = 0.30 for the optimized improvement in *BCR* at a given *s/B* ratio. It is worth mentioning here that a similar recommendation regarding the optimum value of *h/B* was reported by the former studies [25, 29, 32, 50].

Fig. 11 Effect of spacing between successive reinforcements on the load-settlement profile of the footing
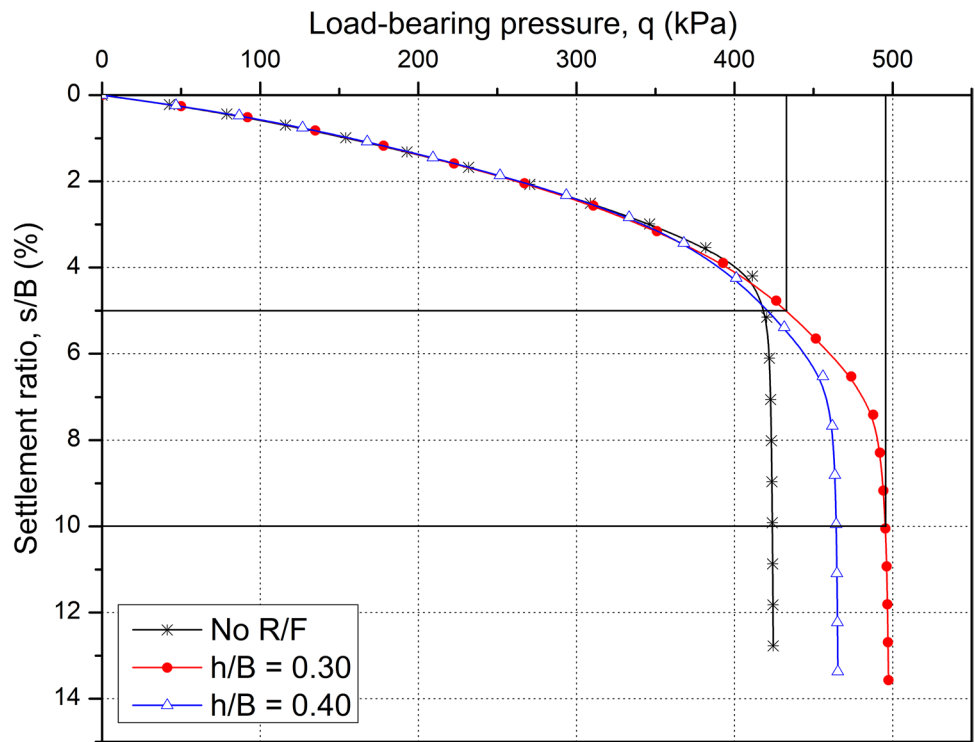

Furthermore, the length and the height of the wrapping ends of the geogrid reinforcement (i.e., l and d) have been varied while keeping b/B, and u/B at 3, and 0.25, respectively. For the case $h/B = 0.30$, the configuration $d/B = 0.30$ is not feasible, as discussed earlier (refer Fig. 1). Therefore,

only to understand the effect of l/B on the $q_{ult, R}$, h is taken as $0.4B$. The outcomes of the load-settlement curve for varying d/B and l/B are presented in Figs. 12 and 13, respectively, which shows that for $s/B > 3\%$, the reinforcement of sand bed by utilizing the wrapping technique has enhanced the

Fig. 12 Variation of load-bearing pressure versus settlement ratio for various d/B ratios
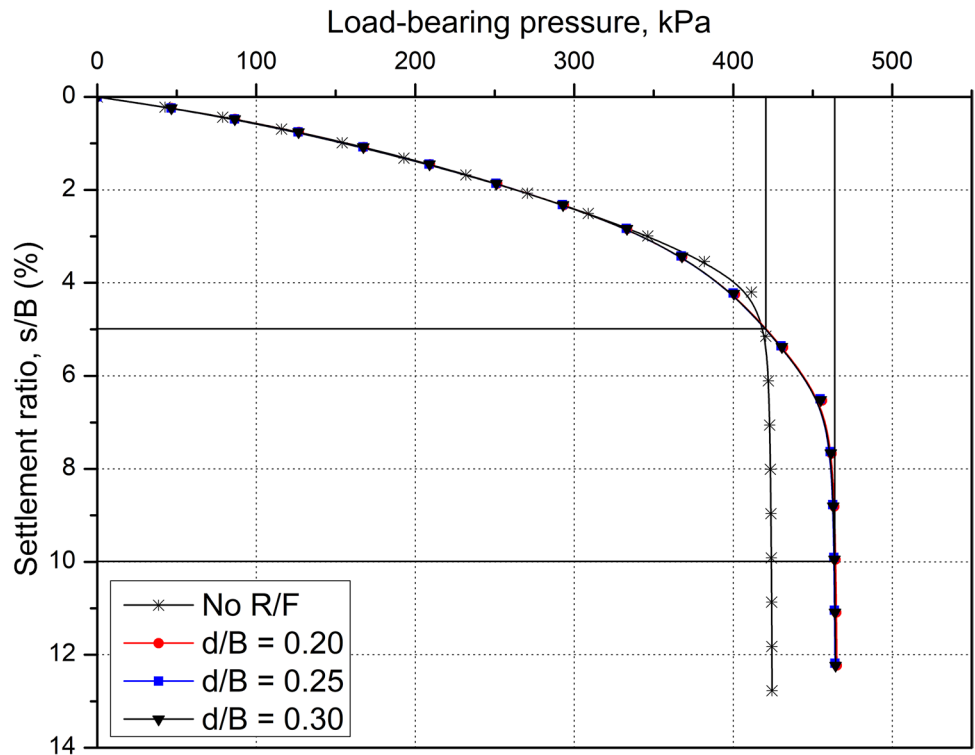
Fig. 13 Variation of load-bearing pressure versus settlement ratio for various l/B ratios
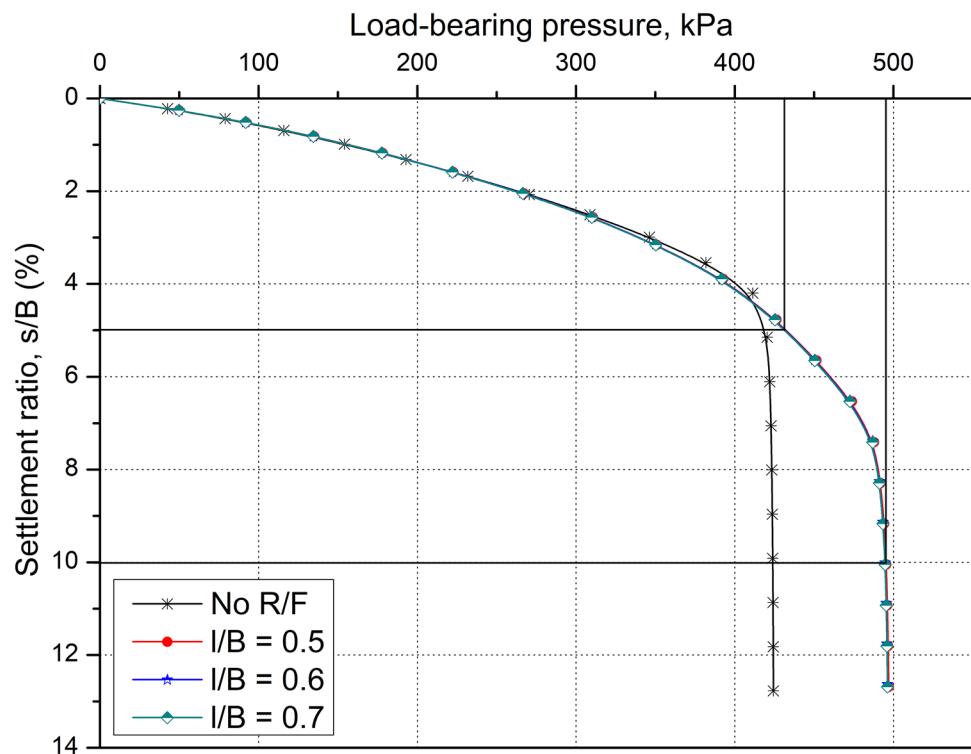
load-settlement characteristics of the footing. However, any change in the d/B and l/B ratios does not affect the improvement in $q_{ult, R}$ significantly, which is noteworthy from the curves that are closely spaced with each other (refer Figs. 12 and 13). This can be inferred that l/B must be provided sufficiently to wrap the ends of geogrid for the confinement, which restricts the movement of soil mass away from the center of the footing, and hence intensifying the improvement in $q_{ult, R}$.

An important mechanical property of the reinforcement, axial elastic stiffness (EA) is the foremost material property of geogrid that is needed to be considered while designing any foundation [13, 40]. Careful selection of geogrid with suitable EA may enhance the BCR with the given reinforcement configuration. To evaluate the significance of the elastic stiffness, a parametric study is conducted on the $q_{ult, R}$, by varying the magnitude of EA as 1000 kN/m, 2000 kN/m, 5000 kN/m, 7000 kN/m, 8500 kN/m, and 10,000 kN/m, and the curves obtained for load-settlement response has been plotted and shown in Fig. 14. Obtained curves indicate that for the normalized settlement ratio of the footing (s/B) < 3%, the curves are closely spaced and as it extends further, a noticeable change is observed in the load-bearing pressure (q). The noted results from the numerical simulations state that on increasing EA from 1000 kN/m to 5000 kN/m, the load-settlement curve changes drastically. However, beyond the value of $EA = 5000$ kN/m, the curves remain virtually constant, and the gap between the curves diminishes owing to the fact that load-settlement curves are not affected by

further increasing the elastic stiffness of the geogrid. It is noticed that, at $s/B = 10\%$ $q_{ult, R}$ is improved by 17.8%, 36.3%, 61.6%, 61.8%, 62.5%, and 63% at $EA = 1000$ kN/m, 2000 kN/m, 5000 kN/m, 7000 kN/m, 8500 kN/m, and 10,000 kN/m, respectively. The results show that for geogrid having $EA > 5000$ kN/m, the difference in the improvement percentage of $q_{ult, R}$ is negligible, henceforth it can be concluded that $EA = 5000$ kN/m is appropriate for the case considered in this study. The possible reason behind the above-noted behavior may be due to the failure of the soil-geogrid interface at higher loads. Even though the soil bed gets stiffer with the use of geogrid with $EA > 5000$ kN/m, but a prior failure of the soil-geogrid interface does not let the footing stand with the higher applied load and leading to the failure of the foundation much earlier than expected.

In a similar study, for a smaller size of footing, Benmebarek et al. [40] and Jaiswal et al. [41] had reported that $EA = 1000$ kN/m is adequate, and with further increment in the magnitude of the elastic stiffness of geogrid, no improvement in $q_{ult, R}$ was reported. From the results obtained in the present study, this can be endorsed that the elastic stiffness (EA) of the geogrid is greatly affected by the footing width. Therefore, it is essential to study the behavior of reinforcing elements before designing a wide foundation.

Thereafter, the variation of the bearing capacity ratio, BCR with elastic stiffness, EA of the reinforcing material is also studied and presented in Fig. 15. For $s/B = 5\%$, the improvement in BCR is linear from $EA = 1000$ kN/m to 2000 kN/m, but a sudden increase in BCR was noted at

Fig. 14 Effect of elastic stiffness of the geogrid, *EA* on the ultimate load-bearing capacity of reinforced soil mass, $q_{ult,\,R}$
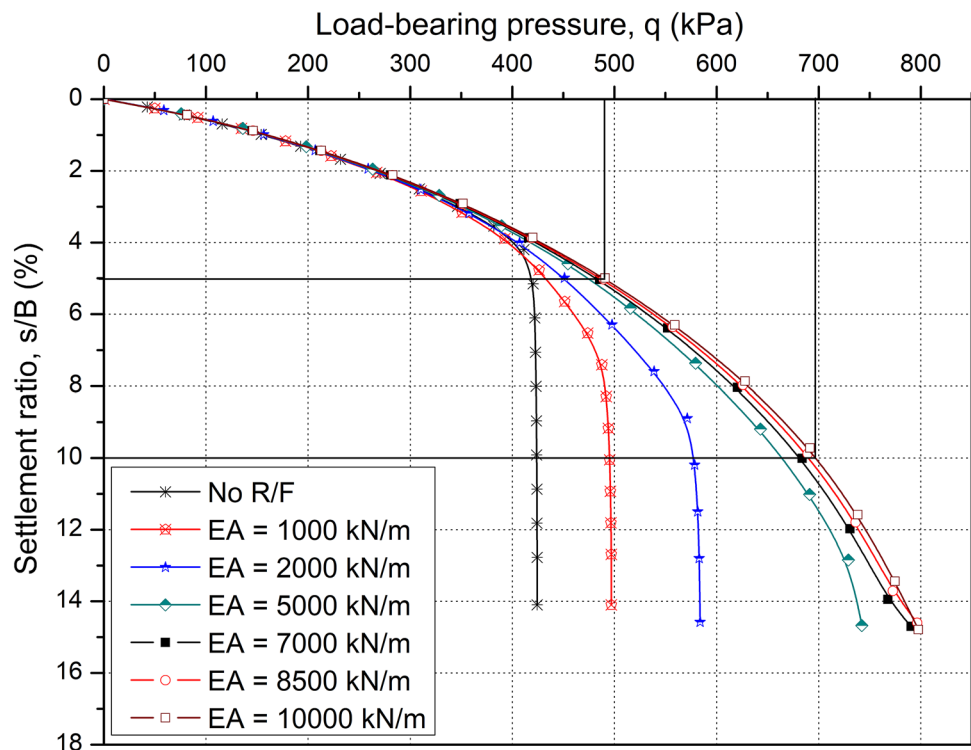
EA = 5000 kN/m, though with further increase in *EA* from 5000 to 10,000 kN/m, *BCR* remains invariable. An improvement of 5.7% and 34.2% is reported in *BCR* corresponding to *EA* = 5000 kN/m at *s/B* = 5% and 10%, respectively.

The deformation shape of the failed soil mass is observed for varying *EA* of the geogrid and the incremental displacement vector field beneath the footing is examined (as shown in Fig. 16). Figure 16a demonstrates the displacement vectors for unreinforced foundation bed beneath the footing, similar to the observation reported by Aria et al. [46]. The displacement vectors at the soil-geogrid interface in Fig. 16b–d, shows that the vertical movement of the soil beneath the footing is hindered by the high tensile member, and the lateral displacement of soil mass enclosed in the geogrid is resisted by the wrapping ends of the reinforcement. This confinement effect is being introduced with the presence of friction at the soil-geogrid interface, as reported by Sharma et al. [64]. However, the results indicate that the density of the displacement vectors beneath the second and third layers of reinforcement decreases due to an increase in the elastic stiffness of the geogrid. This may be attributed to the fact that increasing the elastic stiffness (*EA*) of the geogrid reinforcement creates a stiffer soil bed which dissipates the displacement of the soil mass with depth below the footing and restricts the major displacement vectors near the footing only.

The displacement contour of the soil mass in the vertical direction for unreinforced earth bed and the best configuration in the reinforced case obtained from the present study is shown in Fig. 17a and b, respectively, which primarily demonstrate the migration of the soil particles from their original place. Zone I show the maximum movement of the soil particles, while zone I disperse into zone II, which shows the reduction in soil movement. The maximum displacement is observed in the lateral direction, i.e., both sides of the footing. However, in the unreinforced case (i.e., Fig. 17a) the extent of displacement contour beneath the footing ranges up to a depth of 1.5–1.8 *B*, whereas in the reinforced case (i.e., Fig. 17b) the extent of displacement is noticeable up to a depth of 0.8*B* to 1.0*B*. Although this displacement is observed in the case when yielding of both the soil and the geogrid begins to happen, which makes it more convenient to understand the improvement in soil behavior. Figure 17 sheds light on the enhancement of load-settlement characteristics of the footing resting on the reinforced earth bed using geogrid with wraparound technique.

Analysis of generalized stress and strain distributions in the case of reinforced and unreinforced earth beds can justify the existence of a critical zone of soil mass that is influenced by the installation of reinforcement. The stresses transmitted into the foundation bed due to footing load can be obtained from the load-transfer mechanisms and using elasticity theory or Schmertmann's strain influence factor (I_z) [65]. Figure 18a shows the profile of normalized vertical strain (ε_{yy}/q_u) to the normalized depth (*z/B*) for a strip footing (*z* is the depth measured from ground level). Schmertmann et al. [65] proposed that for strip footing, the peak value of strain occurs near 1.0*B* and it converges to almost zero at

Fig. 15 Variation of bearing capacity ratio (*BCR*) with axial elastic stiffness of the geogrid (*EA*) at *s/B* = 5% and 10%
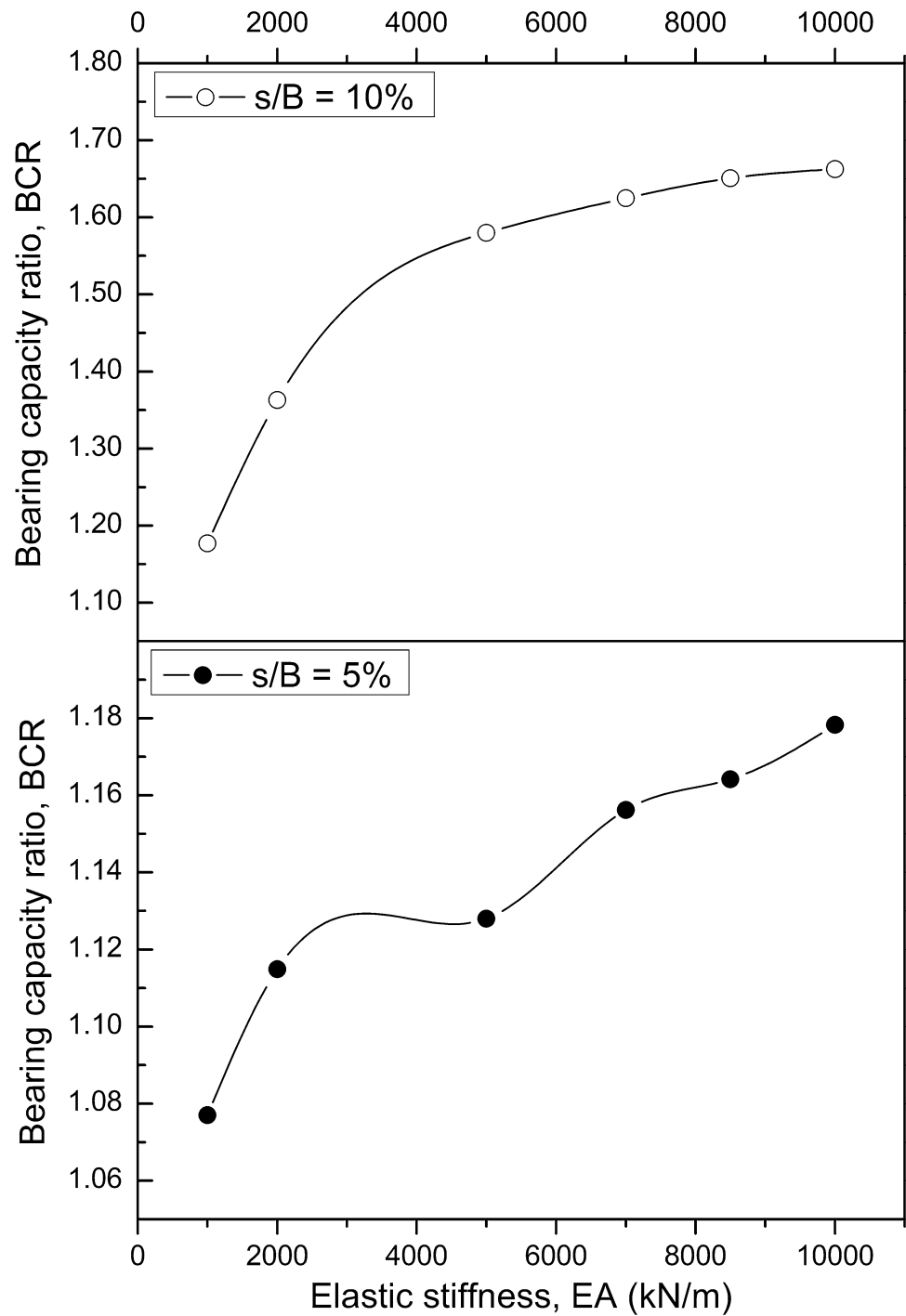
a depth of *4B* from the footing. The simulations from the present study also affirmed similar outcomes as suggested by Schmertmann et al. [65], i.e., the peak value of strain occurs at 0.80*B* for the unreinforced case. Whereas in the case of reinforced soil mass below footing with geogrid having *EA* = 1000 kN/m, the peak normalized strain is reduced by 40% when compared to unreinforced case but it occurs exactly at *z/B* = 1.0, which is similar to the findings of Schmertmann et al. [65]. Furthermore, with increases in

the elastic stiffness of the geogrid (*EA*) from 1000 kN/m to 5000 kN/m, the peak value of ε_{yy}/q_u kept on intensifying and amplified by 18.4% at *EA* = 5000 kN/m but the location of peak normalized strain is observed to be shifted above at *z/B* = 0.60.

For creating a better understanding of the stresses beneath footing, the variation of normalized vertical stress (σ_{yy}/q_u) with normalized depth (*z/B*) is also studied and shown in Fig. 18b. It is noticed that with the use of the reinforcement

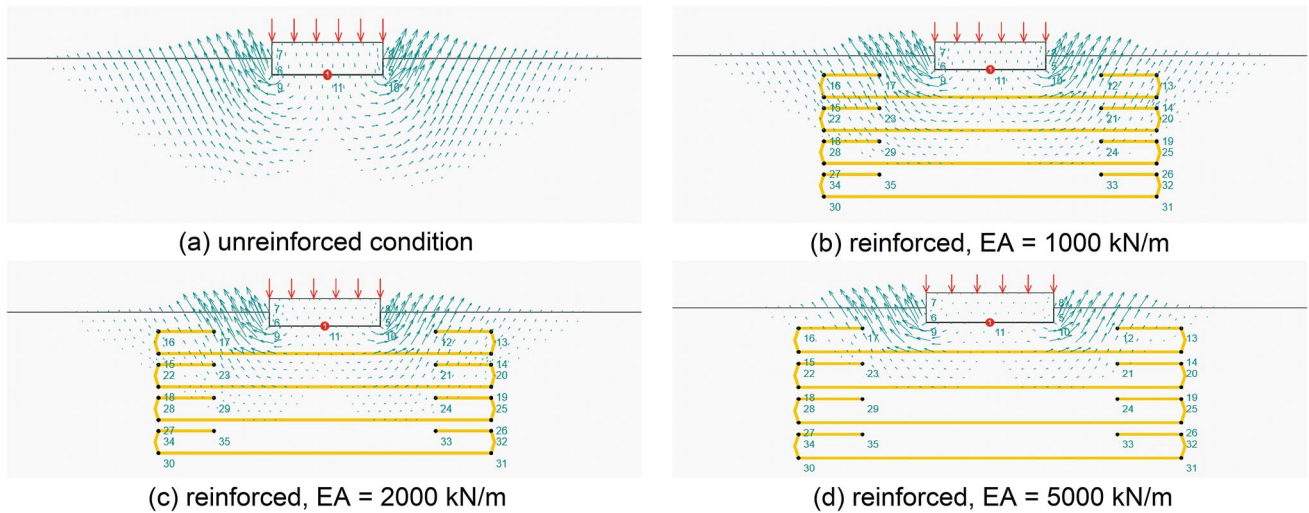**Fig. 16** Displacement vectors of reinforced earth bed using various elastic stiffness of the geogrid, *EA*
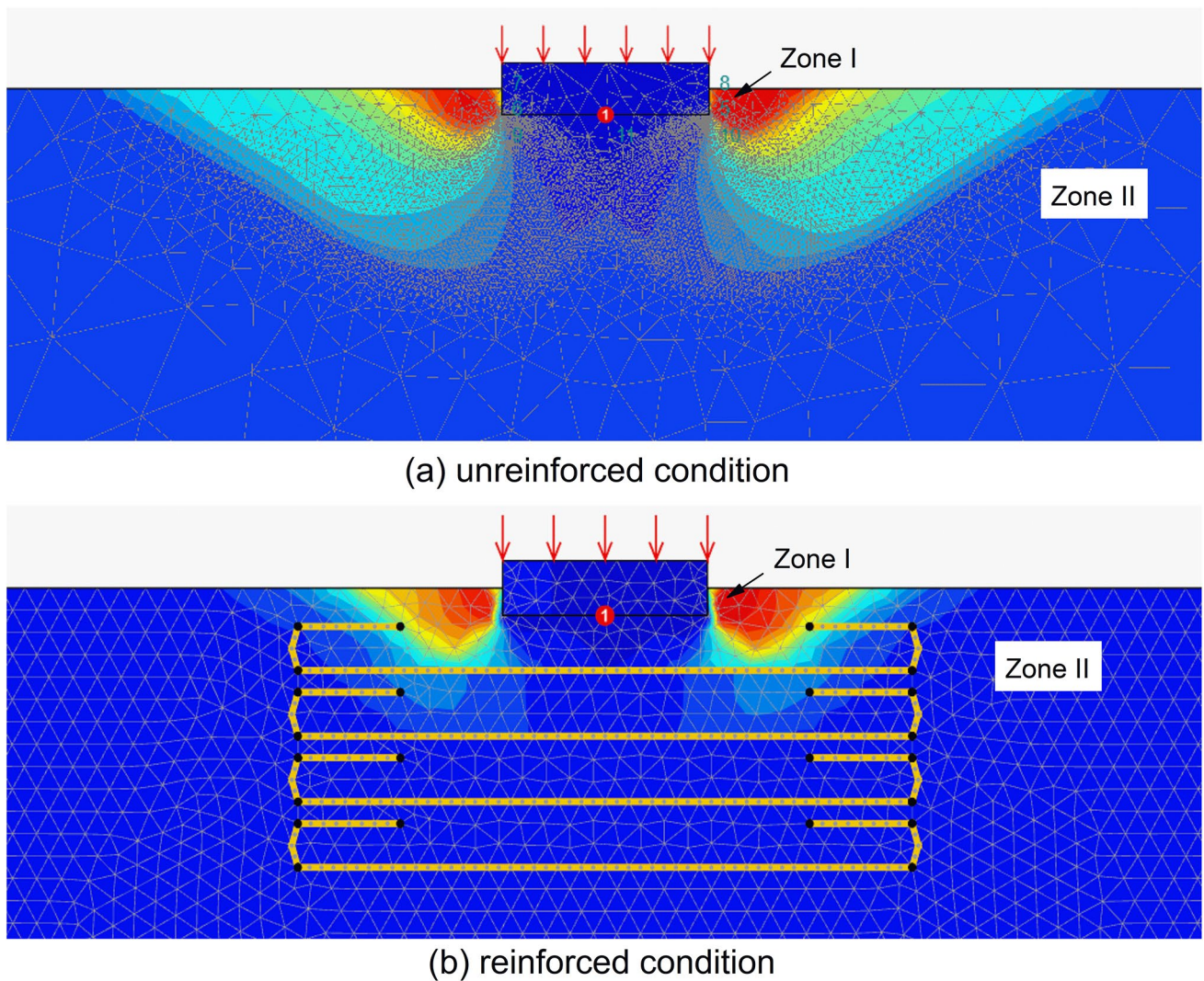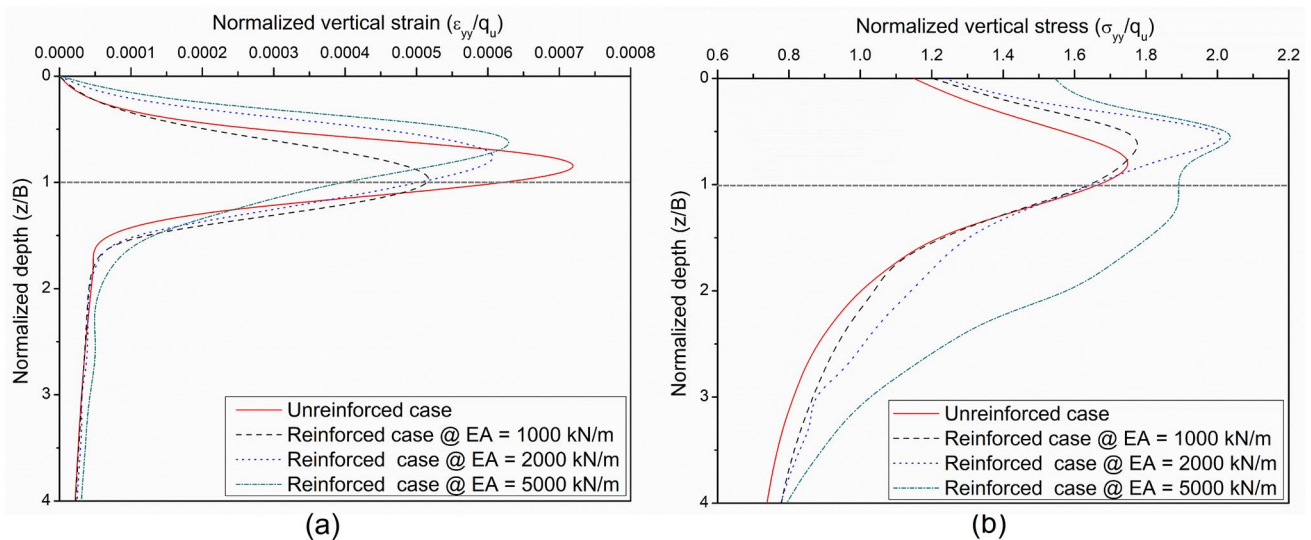

Fig. 17 A look up into the vertical displacement contour of soil mass **a** unreinforced soil mass; and **b** reinforced soil mass

Fig. 18 Variation of **a** normalized vertical strain (ε_{yy}/q_u); and **b** normalized vertical stress (σ_{yy}/q_u) with the normalized depth (z/B)

in the soil mass, not only the σ_{yy}/q_u tends to increase from 1.75 to 1.82, but also the location of peak normalized strain reallocates from 0.75B to 0.5B. The fact that increasing the elastic stiffness up to a certain extent also contributes towards the improvement of the $q_{ult, R}$ can be confirmed in Fig. 18b. Also, EA of the geogrid plays a crucial role in the determination of σ_{yy}/q_u, as an increase in EA from 1000 kN/m to 2000kN/m, the maximum σ_{yy}/q_u improved by 19.3%, and the location of normalized strain reaches a z/B lesser than 1, i.e., approximately 0.8. The maximum value of σ_{yy}/q_u is noted at $EA = 5000$ kN/m, at $z/B = 0.60$, at which the ε_{yy}/q_u is maximum.

The above discussion emphasized that the variation in the distribution of vertical stress and strain beneath the footing indicates that the main mechanism behind the improvement in BCR or $q_{ult, R}$ is by transferring the load offered by the footing deeper into the soil.

Conclusions

The ultimate load-bearing capacity for a 4 m wide strip footing in reinforced (i.e., $q_{ult, R}$) and unreinforced conditions (i.e., q_{ult}) is investigated using the adaptive finite element analysis. This study examines the optimum parameters of reinforcement by adapting the wraparound ends technique for the improvement in the ultimate bearing capacity using a non-dimensional parameter, bearing capacity ratio (BCR). For creating a better understanding of the results, the potential failure envelopes are also studied.

Based on the results obtained from the numerical analysis, the following conclusions can be made on the behavior of wide strip footing resting on soil mass reinforced with multiple layers of geogrid with wraparound ends:

(1) The optimum width of reinforcement (b) for the case considered in this study is about three times the footing width, and the maximum BCR is observed at $b/B = 3$. The potential failure plane in the lateral direction is restrained by the presence of the wrapped ends signifying the full utilization of the reinforcement. Even with the nominal reinforcement (i.e., $EA = 1000$ kN/m), an improvement of almost 18% is noticed at $s/B = 10\%$, when compared to q_{ult}.

(2) The optimum depth of the first layer (u) and vertical spacing between successive layers of reinforcements (h) are recommended as 0.25B and 0.3B, respectively, beyond which the effectiveness of the geogrid be likely to decrease. Also, a minimal overlapping (l) of 0.5B and vertical length of wrapping ends (d) of 0.2B is recommended to maximize the improvement in the bearing capacity.

(3) Apart from the layout and configuration of the reinforcement, elastic stiffness of the reinforcing material (EA) plays an important role in governing the load-settlement behavior of the reinforced earth bed. The $EA = 5000$ kN/m is found to be suitable for maximizing the improvement in $q_{ult, R}$ of almost 62% than q_{ult}. Also, the displacement vectors for this case is noticed to be obstructed completely by the high tensile member.

(4) The extent of the vertical displacement of the soil mass in the unreinforced condition is noticed to be 1.5–1.8 times the footing width (B), however, for the optimum parameters derived for the reinforced case in the present study, the extent of the vertical displacement is

observed to be reduced up to a depth of 0.8–1.0 times B below the footing. Additionally, it is found that the peak normalized vertical strain (ε_{yy}/q_u) and peak normalized vertical stress (σ_{yy}/q_u) for the reinforced case occur at a depth of $0.5B$ below the footing.

Declarations

Conflict of Interest On behalf of all authors, the corresponding author states that there is no conflict of interest.

References

1. Badakhshan E, Noorzad A (2017) Effect of footing shape and load eccentricity on behavior of geosynthetic reinforced sand bed. Geotext Geomembranes 45(2):58–67. https://doi.org/10.1016/j.geotexmem.2016.11.007
2. Biswas A, Krishna AM, Dash SK (2016) Behavior of geosynthetic reinforced soil foundation systems supported on stiff clay subgrade. Int J Geomech 16(5):1–15. https://doi.org/10.1061/(ASCE)GM.1943-5622.0000559
3. Chakraborty D, Kumar J (2014) Bearing capacity of strip foundations in reinforced soils. Int J Geomech 14(1):45–58. https://doi.org/10.1061/(ASCE)GM.1943-5622.0000275
4. Chen Q, Abu-Farsakh M (2015) Ultimate bearing capacity analysis of strip footings on reinforced soil foundation. Soils Found 55(1):74–85. https://doi.org/10.1016/j.sandf.2014.12.006
5. Chen Q, Abu-Farsakh M, Sharma R (2013) Laboratory investigation and analytical solution to the behavior of foundations on geosynthetic reinforced sands. Sound Geotech Res Pract. https://doi.org/10.1061/9780784412770.024
6. Rowe KR, Skinner GD (2001) Numerical analysis of geosynthetic reinforced retaining wall constructed on a layered soil foundation. Geotext Geomembranes 19(7):387–412. https://doi.org/10.1016/S0266-1144(01)00014-0
7. Sharma RS, Kumar BRP, Nagendra G (2004) Compressive load response of granular piles reinforced with geogrids. Can Geotech J 41(1):187–192. https://doi.org/10.1139/t03-075
8. Rowe RK, Taechakumthorn C (2008) Combined effect of PVDs and reinforcement on embankments over rate-sensitive soils. Geotext Geomembranes 26(3):239–249. https://doi.org/10.1016/j.geotexmem.2007.10.001
9. Stuedlein AW, Holtz RD (2013) Bearing capacity of spread footings on aggregate pier reinforced clay. J Geotech Geoenvironmental Eng 139(1):49–58. https://doi.org/10.1061/(asce)gt.1943-5606.0000748
10. Nicks JE, Esmaili D, Adams MT (2016) Deformations of geosynthetic reinforced soil under bridge service loads. Geotext Geomembranes 44(4):641–653. https://doi.org/10.1016/j.geotexmem.2016.03.005
11. Rahmouni O, Mabrouki A, Benmeddour D, Mellas M (2016) A numerical investigation into the behavior of geosynthetic-reinforced soil segmental retaining walls. Int J Geotech Eng 10(5):435–444. https://doi.org/10.1080/19386362.2016.1158443
12. Zheng Y, Fox PJ (2016) Numerical investigation of geosynthetic-reinforced soil bridge abutments under static loading. J Geotech Geoenvironmental Eng 142(5):04016004. https://doi.org/10.1061/(asce)gt.1943-5606.0001452
13. Kazi M, Shukla SK, Habibi D (2015) An improved method to increase the load-bearing capacity of strip footing resting on geotextile-reinforced sand bed. Indian Geotech J 45(1):98–109. https://doi.org/10.1007/s40098-014-0111-9
14. Shukla SK (2002) Geosynthetics and their applications. Thomas Telford Ltd
15. Shukla SK (2016) An introduction to geosynthetic engineering. CRC Press, New York, London
16. Vidal H (1969) The principle of reinforced earth. Geotech Spec Publ 282:1–16
17. Binquet J, Lee KL (1975) Bearing capacity analysis of reinforced earth slabs. J Geotech Geoenvironmental Eng 101(12):1257–1276
18. Yetimoglu T, Inanir M, Inanir OE (2005) A study on bearing capacity of randomly distributed fiber-reinforced sand fills overlying soft clay. Geotext Geomembranes 23(2):174–183. https://doi.org/10.1016/j.geotexmem.2004.09.004
19. Fragaszy J, Lawton E (1985) Bearing capacity of reinforced sand subgrades. J Geotech Eng 110(10):1500–1507. https://doi.org/10.1061/(ASCE)0733-9410(1984)110:10(1500)
20. Huang CC, Tatsuoka F (1990) Bearing capacity of reinforced horizontal sandy ground. Geotext Geomembranes 9(1):51–82. https://doi.org/10.1016/0266-1144(90)90005-W
21. Dash SK, Rajagopal K, Krishnaswamy NR (2004) Performance of different geosynthetic reinforcement materials in sand foundations. Geosynth Int 11(1):35–42. https://doi.org/10.1680/gein.2004.11.1.35
22. Guido VA, Chang DK, Sweeney MA (1986) Comparison of geogrid and geotextile reinforced earth slabs. Can Geotech J 23(4):435–440. https://doi.org/10.1139/t86-073
23. Basudhar PK, Saha S, Deb K (2007) Circular footings resting on geotextile-reinforced sand bed. Geotext Geomembranes 25:377–384. https://doi.org/10.1016/j.geotexmem.2006.09.003
24. Bera AK, Ghosh A, Ghosh A (2005) Regression model for bearing capacity of a square footing on reinforced pond ash. Geotext Geomembranes 23(3):261–285. https://doi.org/10.1016/j.geotexmem.2004.09.002
25. Tavangar Y, Shooshpasha I (2016) Experimental and numerical study of bearing capacity and effect of specimen size on uniform sand with medium density, reinforced with nonwoven geotextile. Arab J Sci Eng 41(10):4127–4137. https://doi.org/10.1007/s13369-016-2101-y
26. Kazi M, Shukla SK, Habibi D (2015) Behavior of embedded strip footing on sand bed reinforced with multilayer geotextile with wraparound ends. Int J Geotech Eng 9(5):437–452. https://doi.org/10.1179/1939787914Y.0000000085

27. Ghosh A, Ghosh A, Bera AK (2005) Bearing capacity of square footing on pond ash reinforced with jute-geotextile. Geotext Geomembranes 23(2):144–173. https://doi.org/10.1016/j.geotexmem.2004.07.002

28. Khing KH, Das BM, Puri VK et al (1993) The bearing-capacity of a strip foundation on geogrid-reinforced sand. Geotext Geomembranes 12(4):351–361. https://doi.org/10.1016/0266-1144(93)90009-D

29. Omar MT, Das BM, Puri VK, Yen SC (1993) Ultimate bearing capacity of shallow foundations on sand with geogrid reinforcement. Can Geotech J 30(3):545–549. https://doi.org/10.1139/t93-046

30. Yetimoglu T, Wu JTH, Saglamer A (1995) Bearing capacity of rectangular footings on geogrid-reinforced sand. J Geotech Eng 1(1):2083–2099. https://doi.org/10.1061/(ASCE)0733-9410(1994)120:12(2083)

31. Shin EC, Das BM, Lee ES, Atalar C (2002) Bearing capacity of strip foundation on geogrid-reinforced sand. Geotech Geol Eng 20:169–180

32. Chung W, Cascante G (2007) Experimental and numerical study of soil-reinforcement effects on the low-strain stiffness and bearing capacity of shallow foundations. Geotech Geol Eng 25(3):265–281. https://doi.org/10.1007/s10706-006-9109-0

33. Latha GM, Somwanshi A (2009) Bearing capacity of square footings on geosynthetic reinforced sand. Geotext Geomembranes 27(4):281–294. https://doi.org/10.1016/j.geotexmem.2009.02.001

34. Abu-Farsakh M, Chen Q, Sharma R (2013) An experimental evaluation of the behavior of footings on geosynthetic-reinforced sand. Soils Found 53(2):335–348. https://doi.org/10.1016/j.sandf.2013.01.001

35. Kumar J, Sahoo JP (2013) Bearing capacity of strip foundations reinforced with geogrid sheets by using upper bound finite-element limit analysis. Int J Numer Anal Methods Geomech 37(18):3258–3277. https://doi.org/10.1002/nag.2189

36. Shukla SK (2015) Core concepts of geotechnical engineering. ICE Publishing

37. Kazi M, Shukla SK, Habibi D (2015) Effect of submergence on settlement and bearing capacity of surface strip footing on geotextile-reinforced sand bed. Int J Geosynth Gr Eng 1(4):1–11. https://doi.org/10.1007/s40891-014-0006-y

38. Aria S, Shukla SK, Mohyeddin A (2019) Numerical investigation of wraparound geotextile reinforcement technique for strengthening foundation soil. Int J Geomech 19(4):04019003. https://doi.org/10.1061/(asce)gm.1943-5622.0001361

39. Aria S, Shukla SK, Mohyeddin A (2021) Behaviour of sandy soil reinforced with geotextile having partially and fully wrapped ends. Proc Inst Civ Eng - Gr Improv 174(1):29–41. https://doi.org/10.1680/jgrim.18.00102

40. Benmebarek S, Djeridi S, Benmebarek N, Belounar L (2018) Improvement of bearing capacity of strip footing on reinforced sand. Int J Geotech Eng 12(6):537–545. https://doi.org/10.1080/19386362.2017.1309136

41. Jaiswal S, Srivastava A, Chauhan VB (2022) Performance of strip footing on sand bed reinforced with multilayer geotextile with wraparound ends. Ground improvement and reinforced soil structures. Springer, Singapore, pp 721–732. https://doi.org/10.1007/978-981-16-1831-4_64

42. Shin EC, Das BM (2000) Experimental study of bearing capacity of a strip foundation on geogrid-reinforced sand. Geosynth Int 7(1):59–71. https://doi.org/10.1680/gein.7.0166

43. Touahmia M, Rouili A, Boukendakdji M, Achour B (2018) Experimental and numerical analysis of geogrid-reinforced soil systems. Arab J Sci Eng 43(10):5295–5303. https://doi.org/10.1007/s13369-018-3158-6

44. Ouria A, Mahmoudi A, Sadeghpour H (2020) Effect of the geotextile arrangement on the bearing capacity of a strip footing. Int J Geosynth Gr Eng. https://doi.org/10.1007/s40891-020-00219-w

45. Lovisa J, Shukla SK, Sivakugan N (2010) Behaviour of pre-stressed geotextile-reinforced sand bed supporting a loaded circular footing. Geotext Geomembranes 28(1):23–32. https://doi.org/10.1016/j.geotexmem.2009.09.002

46. Aria S, Shukla SK, Mohyeddin A (2017) Optimum burial depth of geosynthetic reinforcement within sand bed based on numerical investigation. Int J Geotech Eng 14(1):71–79. https://doi.org/10.1080/19386362.2017.1404202

47. Jaiswal S, Chauhan VB (2021) Assessment of seismic bearing capacity of a strip footing resting on reinforced earth bed using pseudo-static analysis. Civ Environ Eng Rep 31(2):117–137. https://doi.org/10.2478/ceer-2021-0023

48. Meguid MA, Dang HK (2009) The effect of erosion voids on existing tunnel linings. Tunn Undergr Sp Technol 24(3):278–286. https://doi.org/10.1016/j.tust.2008.09.002

49. Lu M, McDowell GR (2006) Discrete element modelling of ballast abrasion. Geotechnique 56(9):651–655. https://doi.org/10.1680/geot.2006.56.9.651

50. Krabbenhoft K, Lyamin A, Krabbenhoft J (2020) Optum computational engineering <www.optumce.com>

51. Kazi M, Habibi D, Shukla SK, Habibi D (2014) Behaviour of an embedded footing on geotextile-reinforced sand. Proc Inst Civ Eng Gr Improv 169(2):1–14. https://doi.org/10.1680/grim.14.00022

52. Adams MT, Collin JG (1997) Large model spread footing load tests on geosynthetic reinforced soil foundations. J Geotech Geoenviromental Eng ASCE 123(1):66–72. https://doi.org/10.7550/rmb.37002

53. Jaiswal S, Srivastava A, Chauhan VB (2021) Improvement of bearing capacity of shallow foundation resting on wraparound geotextile reinforced soil. In: International Foundations Congress and Equipment Expo 2021. ASCE, GSP 324, Dallas, Texas, pp 65–74. https://doi.org/10.1061/9780784483411.007

54. Pandey A, Chauhan VB (2020) Evaluation of pull-out capacity of helical anchors in clay using finite element analysis. Geo-Congress 2020:60–68. https://doi.org/10.1061/9780784482803.007

55. Srivastava A, Chauhan VB (2020) Numerical studies on two-tiered MSE walls under seismic loading. SN Appl Sci. https://doi.org/10.1007/s42452-020-03414-6

56. Jaiswal S, Chauhan VB (2021) Response of strip footing resting on earth bed reinforced with geotextile with wraparound ends using finite element analysis. Innov Infrastruct Solut 6(2):1–9. https://doi.org/10.1007/s41062-021-00486-0

57. Liu Y, Glass G (2013) Effects of mesh density on finite element analysis. SAE Tech Pap 2:1–7. https://doi.org/10.4271/2013-01-1375

58. Durga Prasad B, Hariprasad C, Umashankar B (2016) Load-settlement response of square footing on geogrid reinforced layered granular beds. Int J Geosynth Gr Eng 2(36):1–10. https://doi.org/10.1007/s40891-016-0070-6

59. Tafreshi SNM, Dawson AR (2010) Comparison of bearing capacity of a strip footing on sand with geocell and with planar forms of geotextile reinforcement. Geotext Geomembranes 28(1):72–84. https://doi.org/10.1016/j.geotexmem.2009.09.003

60. El Sawwaf M, Nazir AK (2010) Behavior of repeatedly loaded rectangular footings resting on reinforced sand. Alexandria Eng J 49(4):349–356. https://doi.org/10.1016/j.aej.2010.07.002

61. Terzaghi K (1943) Theoretical soil mechanics. John Wiley and Sons, New York, London

62. Buragadda V, Thyagaraj T (2019) Bearing capacity of jute geotextile-reinforced sand bed. Int J Geosynth Gr Eng. https://doi.org/10.1007/s40891-019-0178-6

63. Neves J, Lima H, Gonçalves M (2016) A numerical study on the implications of subgrade reinforcement with geosynthetics in pavement design. Procedia Eng 143:888–895. https://doi.org/10.1016/j.proeng.2016.06.151

64. Sharma R, Chen Q, Abu-Farsakh M, Yoon S (2009) Analytical modeling of geogrid reinforced soil foundation. Geotext Geomembranes 27(1):63–72. https://doi.org/10.1016/j.geotexmem.2008.07.002

65. Schmertmann JH, Hartman JP, Brown PR (1978) Improved strain influence factor diagrams. J Geotech Eng Div 104(8):1131–1135